2009 American Control Conference
Hyatt Regency Riverfront, St. Louis, MO, USA
June 10-12, 2009

Optimal design and operation of a multiscale GaAs/AlAs deposition process

Christopher M. Behrens and Antonios Armaou[†], *Senior Member, IEEE & Member, AIChE*

***Abstract*— We consider optimal operating conditions of a gallium arsenide/aluminum arsenide (GaAs/AlAs) deposition process with objectives of uniform deposition of the film heterostructure across the wafer surface at the macroscopic scale and the interfacial uniformity of the GaAs/AlAs heterostructure at the microscopic scale. We use a finite element solver to determine macroscale solutions and kinetic Monte Carlo (kMC) techniques to determine the mesoscale solution of the problem. We characterize the interfaces between species and apply the simulation methodology to a multiscale optimization framework to minimize the interfacial step densities while also minimizing temperature, annealing time, and maximizing thickness uniformity. The design variables are temperature, annealing time, precursor concentration, and input velocity. In order to reduce the prohibitive computational expense of the function evaluations, we employ an in situ adaptive tabulation scheme around the mesoscale inputs. The resulting optimization problem combined with this methodology becomes computationally tractable, and is able to increase the thickness uniformity and maintain low interfacial step densities.**

I. INTRODUCTION

Continuous pressure on profit margins and reducing costs has recently led to a move towards process optimization. A corresponding increase in computational power has resulted in the development of computational models that can be used in optimization of spatially distributed multiscale systems. The term multiscale can have multiple definitions; in this work it refers to systems where the mathematical descriptions to model them need to account for phenomena that span length scales that differ over several orders of magnitude. These descriptions can cover the smallest (quantum, atomistic, molecular, microscale) to the intermediate (mesoscale, kMC, Lattice-Boltzmann) to the largest (macroscale, continuum) regimes [1]. Methodologies used to determine solutions in one length scale regime are frequently not suitable in another regime, either as they do not capture the required level of detail or are computationally infeasible. As a result, spatial multiscale models, which make use of appropriate methodologies for solving systems at each length scale involved and then intimately connect the solutions, have been developed. Examples that combine macroscale and mesoscale techniques have been used in [2] for gas-phase data, film morphology, and in [3] and [4] to model thin-film growth and catalytic oxidation of CO. Solving these systems, however, can often require extensive computational overhead, due to simulation time, possible iterative procedures at all involved length scales to achieve convergence, and several iterations for multiscale optimization using black-box algorithms such as Nelder-Mead or Hooke-Jeeves. Methods to reduce the computational cost of simulations at various length scales and the entire framework include replacement of the associated partial differential equation (PDE) systems with low-order ordinary differential equation (ODE) systems derived from the method of weighted residuals [3] [4] [5], coarse-graining of kinetic Monte Carlo schemes [6] and timesteppers from equation-free computing [7] [8] [9], applying filters [10], using configurations with the greatest contributions [11], multi-step methods [12], using mathematically-supported linear interpolation from previously tabulated results instead of simulation when possible [3] [4], and recreation of surfaces with properties that approximate a simulated surface [13]. We maintain that such methodologies can be applied towards the optimal operation of microelectronics fabrication processes, such as metal organic vapor phase epitaxy (MOVPE).

MOVPE is one method used to grow thin films for use in manufacturing for various microelectronic applications. These films typically have thicknesses on the order of a few microns (roughly $10^2 - 10^3$ molecules.) To obtain maximum performance, mesoscale regime properties, such as the smoothness of thin-film surfaces and interfaces between layers of films comprised of multiple components, may require optimization. The mesoscale regime exists at a length scale somewhat larger than required for individual molecules, yet sufficiently small that continuum equations cannot be applied. In [13], a multiscale optimization framework was developed to determine optimal processing conditions for a gallium nitride (GaN) system. This work extends the results of [3], [13], and [4] to a layered heterostructure consisting of alternating layers of gallium arsenide (GaAs) and aluminum arsenide (AlAs.) In addition to the increase in complexity due to the introduction of additional species, layered heterostructures also require accounting for properties along multiple interfaces, which first must be characterized. We present a multiscale model that outlines characterization and calculation of interfacial properties. We use a finite-element solver for the macroscopic reaction-transport equations and kMC simulations to simulate the atomistic evolution of the film. In order to reduce computational overhead, we employ in situ adaptive tabulation (ISAT) to reduce the number of required simulations.

Financial support from the National Science Foundation, CAREER Award # CBET 06-44519, and American Chemical Society - Petroleum Research Fund Research Initiation Award #PRF 44300-G9, is gratefully acknowledged.

[†]Department of Chemical Engineering, The Pennsylvania State University, University Park, PA 16802, USA, Tel: (814) 865-5316, Email: armaou@engr.psu.edu.

978-1-4244-4524-0/09/$25.00 ©2009 AACC

II. MACROSCALE MODEL

Metal organic vapor phase epitaxy (MOVPE) is a technique that has become widely used in semiconductor production [14]. Frequently, precursors enter from separate inlets at the top of a multiple-inlet reactor to avoid premixing. Upon entering the reactor, these species may undergo chemical reactions to form the reactants which must be accounted for in overall and species mass transport equations. Both the original reactants and newly formed species are then deposited onto a wafer surface, although much of the material will eventually be exhausted through an outlet. At the wafer surface, adsorption, desorption, surface diffusion, and additional chemical reactions can occur, although during deposition desorption is usually negligible. The ultimate result is that the molecules are deposited on a surface, growing a thin film. For films consisting of multiple layers of different species, however, different precursors need to enter the reactor at different times.

The reaction-transport mechanism that governs the behavior of the reactor is determined from a system of PDEs that describe energy transport, momentum transport, and species mass transport. These PDE systems include the material property parameters of density, viscosity, thermal conductivity, heat capacity, and diffusion coefficients, most of which are functions of temperature. Also important are reaction rates, which are functions of temperature and species concentrations. The reactor used to produce the desired product usually has a showerhead configuration, and is presented in Figure 1. We use cylindrical geometry to model this reactor. We assume no dependence upon angular position, simplifying the PDE to a two-dimensional description. Due to rapid clearing of one species to the next upon change in deposition compared to the duration of the deposition process, quasi steady-state conditions are also assumed. The transport-reaction equations used are:

$$\nabla \cdot (-k\nabla T) = -\rho C_p \mathbf{u} \cdot \nabla T \tag{1}$$

$$\nabla \cdot (-D_i \nabla C_i) = R_i - \mathbf{u} \cdot \nabla C_i, \quad i = 1...m \tag{2}$$

$$\rho \mathbf{u} \cdot \mathbf{u} = \nabla \cdot [-PI + \mu(\nabla \mathbf{u} + (\nabla \mathbf{u})^T)] \tag{3}$$

where T is the temperature, C_i is the concentration of m species i, u is the velocity vector, k is the thermal conductivity, ρ is the density, C_p is the heat capacity, D_i is the diffusivity for species i, R_i is the reaction rate for species i, μ is the dynamic viscosity, P is the pressure, and I is the identity matrix. Axial symmetry boundary conditions can be applied when r=0. Walls are handled with insulation and no-slip conditions. Dirichlet boundary conditions are used at the inlet and Neumann boundary conditions are used for the outlet. At the wafer surface, we use no-slip boundary conditions for momentum, Dirichlet boundary conditions for temperature, and Robin boundary conditions for concentration (which represents the surface reactions.) Process inputs for this problem are temperature, velocities of the inlet streams, and concentrations of reactants. We used the commercially available COMSOL software as a finite element solver for determining the deposition rates along various points on the wafer surface to connect with the mesoscale kMC simulations.

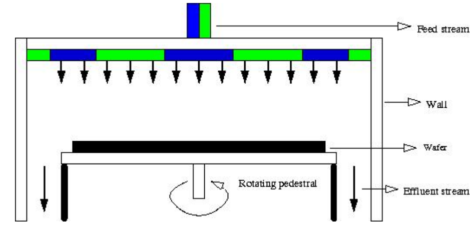

Fig. 1. Schematic of proposed reactor.

III. MESOSCALE MODEL

The deposition rates for GaAs and AlAs obtained from the solution of the macroscopic PDE system and the temperature enter a mesoscale kMC simulation. Also entering into the mesoscale kMC simulations are deposition time and annealing time, a period when no species are deposited and only nearest neighbor migrations can occur. These kMC simulations then calculate several important microscopic properties of the film. Events in kMC simulations have been shown to follow a Poisson process [15], which accurately describes the deposition process.

One challenge associated with applying a layered heterostructure deposition problem towards an optimization framework is characterization of the film surface and multiple interfaces. To characterize the smoothness of a surface, the measure of roughness is often used. Two different sources of roughness include root-mean-square (RMS) roughness, derived from the autocorrelation function (ACF), and roughness derived from the height-density correlation function (HDCF.) Further descriptions can be found in [13]. An alternative method for characterizing interfacial smoothness is step density. For a cubic solid-on-solid model (SOS), step density S (when the azimuthal angle $\phi = 0$) is defined as:

$$S = L^{-1} \sum_{i,j} (1 - \delta(h_{i,j}, h_{i+1,j})) \tag{4}$$

where δ is the Kronecker delta function, $h_{i,j}$ is the height of lattice site (i,j), and L is the number of lattice sites [16].

Step density can be measured as either a function of time or space. When measured as a function of time, the step density of the surface is calculated continuously as the process evolves; this metric can be measured and used for control. Deposition of a particular species will eventually result in obtaining a stationary state value for step density in time which will vary only slightly due to stochastic noise and because lattice heights take on discrete values. The particular stationary state value obtained depends on the species currently being deposited, the temperature, and the deposition rates. Interestingly, the property of an equilibrium value can quite easily be exploited in reducing computation time for obtaining step density information, since step density is independent of absolute film thickness. As a result, we can perform simulations for a shorter (thick enough that the the stationary state value has been reached) intermediate layers, as long as we attain layers with step density of zero in space.

Step density can also be calculated at the end of the process as a function of film molecular layer number. We use the same form as in Eq. 4, except instead of heights, we observe any changes in species. The use of this metric is more applicable to the current optimization problem, since we consider steady-state operation and want to optimize the overall process behavior. Thus, we use step density as a function of space (or layer number) in the objective function. Step density in time and in space are affected similarly by changes in temperature and annealing time and for most purposes can be considered interchangeable, although the latter is considerably more computationally efficient.

The main reason we use step density as the metric to characterize interfacial properties of the thin film is due to "bubble" formation. These occur when at an interface, molecules of one species become trapped between molecules of another species in all directions, thus creating an isolated structure which in this work we call a "bubble." Such layer mixing phenomena have been observed in layered heterostructure systems [17]. RMS roughness and roughness calculated from HDCF depend on the average height of the interface, which is unclear when "bubbles" are present. With step density, only the number of changes between adjacent molecules are important, regardless of the composition of the species. As a result, "bubble" formation does not cause any confusion when calculating step density. Step density is also a suitable metric for industrial applications, as it can be measured experimentally through RHEED data [16].

Specifically for the process under consideration, mesoscale kMC simulations are performed using a cubic solid-on-solid (SOS) model assuming perfect overlap and no overhangs. Each event can correspond to two possible outcomes - a GaAs or AlAs molecule can be adsorbed onto the surface, thereby growing the lattice, or it can migrate to an immediately neighboring site. The likelihood of an event being a migration is dependent upon the number of nearest neighbors a molecule has. Each molecule has twelve neighbors outlined in Table I. Migration rates for GaAs/AlAs based on the number of nearest neighbors can be found in [18], with [19] providing values for important constants and prefactors. Note that the model in [18] is for a Zincblende lattice and considers only the migration of the metal species; however, we make the assumption that the migration of total species can be approximated by the migration of metal species, therefore facilitating using a simplified cubic SOS model. Deposition is performed on a three-dimensional lattice, with integer representation for each species. Periodic boundary conditions are assumed for the lattice in order to prevent conditions at the edges from being different than closer to the center. In order to reduce stochastic noise to a workable level and to ensure reasonable results, the size of the lattice used in the simulations should have length and width dimensions of at least 100 by 100. To assure the size was sufficiently large, we compared step densities with those predicted from identical operating conditions for larger lattices (250 by 250) and found that the values obtained for a 100 by 100 were within the expected range.

TABLE I

NEAREST NEIGHBORS MODEL: I: X-DIRECTION, J: Y-DIRECTION, K: Z-DIRECTION

Current position	$X_{i,j,k}$
Adjacent (4)	$X_{i-1,j,k}$, $X_{i+1,j,k}$, $X_{i,j-1,k}$, $X_{i,j+1,k}$
Diagonal (4)	$X_{i-1,j-1,k}$, $X_{i-1,j+1,k}$, $X_{i+1,j-1,k}$, $X_{i+1,j+1,k}$
Underneath (4)	$X_{i-1,j,k-1}$, $X_{i+1,j,k-1}$, $X_{i,j-1,k-1}$, $X_{i,j+1,k-1}$

Due to the complexity and size requirements of individual simulations, solving this problem in an optimization framework could quickly become prohibitive. To partially circumvent such high computational demands, we utilized trends in the properties of interest. In addition to using shorter heights than initially requested, which does not affect the prediction of interfacial roughness, we found that regardless of how many layers preceded one interface, interfaces with AlAs over GaAs will all have nearly identical step densities. The same holds true for interfaces with GaAs above AlAs. While this methodology may inaccurately predict interface heights, layer thickness is a strong linear function that can be calculated from macroscale simulations or easily interpolated from the reduced-size macroscale representations. Another approach is the use of interpolation from stored data, implemented in the ISAT approach.

A. *In Situ Adaptive Tabulation*

In situ adaptive tabulation (ISAT) is a computational technique designed to radically reduce the time required to simulate a process by substituting costly simulations with a linear interpolated solution based on previously tabulated results whenever possible. First used in combustion chemistry [20], the ISAT algorithm has been used in the optimization of CO oxidation [4] and GaN thin film deposition [3]. ISAT has shown to be particularly effective for problems with extremely large numbers of calculations, on the order of 10^3 to 10^9. While the number of simulations required in this case is definitely at the low end of this scale, ISAT also performs well when the same region is traversed repeatedly, as is the case in optimization, or several evaluations of unique but similar points are required, such as what occurs with deposition rates for various points along the wafer surface at a constant temperature and for constant annealing time. Descriptions of the ISAT algorithm can be found in [20] and [4]. A brief and mainly qualitative overview of the ISAT algorithm is explained below.

Consider a query point, ϕ_q, which contains all input properties that determine the dynamic evolution of the important solutions of the process of interest. This point can be compared against a previously tabulated point, ϕ_0, based on the distance between them, the sensitivity matrix of the previously tabulated point, and a user-defined error tolerance ϵ_{tol}. Note that if gradient information is unavailable, the sensitivity matrices must be calculated by performing additional simulations with slight perturbations from the initial conditions. If this calculated function is sufficiently small, ϕ_q is said to lie within the ellipsoid of attraction (EOA) of ϕ_q, and the trajectory of ϕ_q can be determined from interpolation

based on information from ϕ_0. If the ϕ_q does not fall within an EOA for any tabulated point, the process is simulated, the sensitivities are calculated, and a new record is added. The EOA can also be grown if the simulation results indicate that the interpolated solution is within an acceptable error tolerance.

ISAT has the advantage that the table is built as the simulations are performed, and therefore potentially expensive pre-construction techniques are not applied. In order to avoid extensive computation effort due to table lookup, ISAT was initially implemented using a binary tree structure. This practice is frequently employed, but it is not necessarily a requirement, particularly when relatively few function evaluations are needed. It should also be noted that implementing ISAT initially incurs additional computational cost by requiring multiple simulations for a single query. The savings occur when a sufficiently large number of queries can be interpolated, such as during a solution of an optimization problem.

ISAT was initially used in deterministic systems; however, its use has been successfully applied to stochastic systems [21], [4]. When using ISAT in stochastic systems, for calculating sensitivity information, the exact same random number sequence must be used. This technique, referred to as finite differences with common random numbers (FDCRN), can be outlined in [22]. This ensures that the any variation in the solutions between the initial and a perturbed input is due to the perturbation itself and not stochastic noise [23]. It should be noted that while FDCRN is necessary for determining the trajectories for the input of ϕ_q and its associated perturbations, different random number sequences are used for different inputs.

IV. Application to Gallium Arsenide/Aluminum Arsenide Deposition

This work extends the applicability of a previously developed multiscale modeling methodology and characterization techniques to a thin film consisting of alternating layers of GaAs and AlAs. Such a layered heterostructure has significant possibilities in industry; one such promising application is in forming Bragg reflectors for use in yellow-green light-emitting diodes [24]. The reflectors require a high level of interfacial smoothness for maximum performance.

The macroscale model for deposition involves the precursors of trimethyl gallium (TMG, $Ga(CH_3)_3$) and trimethyl aluminum (TMA, $Al(CH_3)_3$,) arsine (AsH_3), using hydrogen as a carrier gas entering into a reactor. Arsine is in excess compared to TMG and TMA, and the hydrogen gas concentration is much larger than that of arsine. Reactions may occur in the gas phase before the species reach the wafer for deposition, forming dimethyl ($M(CH_3)_2$) monomethyl (MCH_3,) and "dimethyl hydride" ($MH(CH_3)_2$) species, where the term M represents the Group III metal Ga or Al. We used a gas-phase reaction scheme based on [25]. We were able to simplify this scheme by investigating the relative reaction rates, relative concentrations, and employing quasi steady-state assumptions. For example, it is assumed that due to the speed of such reactions, any hydrogen radical will react immediately with a methyl radical, forming methane. This allows us to eliminate and combine reactions to form the following simplified gas-phase reaction mechanism:

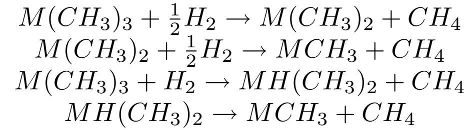

$$M(CH_3)_3 + \tfrac{1}{2}H_2 \rightarrow M(CH_3)_2 + CH_4$$
$$M(CH_3)_2 + \tfrac{1}{2}H_2 \rightarrow MCH_3 + CH_4$$
$$M(CH_3)_3 + H_2 \rightarrow MH(CH_3)_2 + CH_4$$
$$MH(CH_3)_2 \rightarrow MCH_3 + CH_4$$

We found that the concentrations of trimethyl species and the "dimethyl hydride" species are much higher than the monomethyl species, which in turn have a higher concentration than dimethyl species, due to better dissociation than for trimethyl species.

For the surface reaction scheme, since sticking coefficients must be obtained experimentally and may not always be available, we considered the sticking coefficient of all gallium and aluminum containing species to be unity, similar to [5]. We assumed that as arsine is in excess, that any gallium or aluminum metal species that adsorbs onto the surface is immediately covered by an arsenic molecule and forms a metal arsenide layer. Therefore, the flux rate of arsine from the surface is dependent on the flux rates of the metal species. The surface reactions can easily be derived from simple mass balances, and are thus not included here. Since hydrogen is in great excess compared to the deposition of metal species, we assumed that the concentration is constant at the surface for model simplification purposes.

The cylindrical reactor used is modeled in [5] and is shown in Figure 1. The reactor parameters, inlet compositions, and inlet concentrations are outlined in Table II, and the physical properties in Table III, where R is the ideal gas constant and $\overline{M}$ is the average molecular weight. The rates of hydrogen and arsine entering the reactor correspond to a pressure of approximately 0.1 atm. Thermal conductivity, heat capacity, and viscosity were estimated from [26]. Since the macroscale deposition rate outputs are in units of $mol/(m^2 \cdot s)$ and the mesoscale deposition rate inputs are in units of $monolayers/s$, we estimated the number of molecules per layer based on atomic sizes from [27].

TABLE II

Reactor parameters

Radius	5 cm	No. of inlets	3
Height	4.5 cm	Center inlet	3.85 mol/m^3 H_2, TMG or TMA
Inlet spacing	1.25 cm	Middle inlet	3.85 mol/m^3 H_2, 0.6 mol/m^3 AsH_3
Inlet temperature	300 K	Side inlet	3.85 mol/m^3 H_2

TABLE III

Transport parameters

k	$0.0032T + 0.00524$ $[W/(m \cdot K)]$	D	10^{-4} $[m^2/s]$
C_p	$12,000$ $[J/(kg \cdot K)]$	ρ	$\frac{P\overline{M}}{RT}$ $[kg/m^3]$
μ	$10^{-8}(1.959T + 416.31)$ $[Pa \cdot s]$	P	0.1 $[atm]$

The actual model allows for growth of multiple alternating layers of GaAs and AlAs for a particular deposition rate and time at a given temperature, as well as a period of annealing time. During annealing, only next nearest neighbor migrations occur, which implies that the surface of the film evolves towards lower roughness and step density. Increasing the temperature increases the likelihood of molecules overcoming any barriers associated with migration, and therefore move more quickly towards a smoother surface. Increasing deposition rate also increases the step density, as migrations are more likely to compete with deposition events.

V. Optimization Process

We formulated an optimization problem with a microscopic objective of minimizing the interfacial step densities of a thin film consisting of alternating GaAs and AlAs layers across the wafer surface. Although higher temperatures and annealing times will accomplish this goal, higher temperature operation increases the energy associated with the production, and longer annealing times increase processing time, thus reducing production capacity. Since both would reduce profits, we would like to minimize the temperature and annealing time. A macroscopic goal for the optimization problem was to maximize the surface uniformity along the wafer surface. Note that the quality of the film is accounted for through the microscopic objective of reducing the step density of the interfaces across the wafer surface.

We constructed acceptable bounds for temperature, velocity, and concentration. Discontinuous penalties were added for exceeding maximum allowable step densities and exceeding the preset bounds, as well as when algorithmically possible but physically impossible conditions (such as negative annealing times) were obtained. The optimization problem obtained the following form:

$$\begin{aligned} &\min z = T_S^2 + 150A^2 + 12,000(U_G^2 + U_A^2) + P \\ &\qquad\qquad s.t. \\ &P = \begin{cases} 300,000 & S_G > 0.95 \text{ or } S_A > 1.05 \\ 0 & \text{otherwise} \end{cases} \\ &T_S \geq 32,\ T_S \leq 50,\ \ A \geq 0,\ \ C \geq 0.001,\ \ v \geq 0.3. \end{aligned} \tag{5}$$

where T_S is the scaled temperature, $T_S = T/20$, where T is the temperature in Kelvin, A is the annealing time in seconds, U_G and U_A are the surface uniformities of GaAs and AlAs, respectively, P is a discontinuitous penalty, S_G and S_A are the step densities between a lower Ga layer and higher Al layer, and a lower Al layer and higher Ga layer, respectively, C is the concentration of precursor in $\frac{mol}{m^3}$, and v is the inlet velocity in $\frac{m}{s}$. Fifteen sites along the wafer surface were sampled, spaced 0.25 cm apart (obtained from the macroscale part of the multiscale model) to obtain the step density profiles across the wafer surface. This implies that 15 separate kMC simulations must be performed per multiscale simulation if ISAT is not involved. Note that the multiscale model is also part of the constraints of the problem of Eq. 5. Thickness uniformity was calculated using the square root of the sum of the square errors from the mean thickness. In our objective evaluations we disregarded the wafer area closest to the exhaust due to potentially complicated flow patterns that lead to the well known and always unavoidable edge effects. To allow for stochastic variation, the step density allowances can be exceeded three times out of the 15 before the penalty is implemented. While we require that the optimization function is analogous to what should occur in real systems, we recognize that parameters such as weights, penalties, and the decision to make an allowance for three trials exceeding the maximum step density value are tunable parameters. The optimization problem was solved using the Nelder-Mead simplex method via the fminsearch command on MATLAB, where the multiscale simulations were treated as a black box. It is important to note that this particular multiscale system has intrinsic noise due to the mesoscale simulations, and this stochastic noise can often mask small changes in function values due to corresponding changes in input conditions. As a result, global convergence to a single point may not be achievable, but one can obtain near optimal results based on the expectation of the process.

A. Optimization Results

We performed optimization trials at several different initial guesses of operating conditions. A single mesoscale simulation for a given condition is quite time consuming, taking approximately 25 minutes, depending on temperature and deposition time. The process for one ISAT record can take 2 hours, as the simulation must be run five times to determine sensitivity information from perturbations in temperature, annealing time, concentration, and velocity.

The process conditions and step densities for the wafer deposition and the mean step densities across the wafer surface are summarized in Table IV. The AlAs over GaAs step density for this profile was 0.7416, with a GaAs over AlAs step density of 0.9690. The optimal deposition profiles for AlAs over GaAs and for GaAs over AlAs are shown in Figure 2. Also included is the deposition profile at the base case starting condition of 840 K, 5 seconds annealing time, 0.005 $\frac{mol}{m^3}$ precursor, and 0.8 $\frac{m}{s}$. Also shown in Figure 2 is step density as a function of wafer distance from the center. A vertical section of deposition at average wafer deposition conditions is shown in Figure 3, where each box represents a GaAs or AlAs molecule, with the layers of deposition (from bottom) being GaAs, AlAs, and GaAs, respectively.

TABLE IV
OPTIMAL OPERATION CONDITIONS

T	815.8 $[K]$	C	7.2154×10^{-3} $[mol/m^3]$
A	0.3478 $[s]$	v	0.3 $[m/s]$

We observe that for the optimal process operation case outlined here we obtain a profile uniformity of 0.052 for both AlAs over GaAs and AlAs over GaAs. The step densities were maintained just below the threshold before application of the penalties established in Eq. 5, allowing for reductions in both temperature and annealing time. Figure 2 shows that the variation in step density is mainly due to stochastic noise. From Figure 3, we observe that the interfaces are relatively smooth with mainly minor changes in interfacial height.

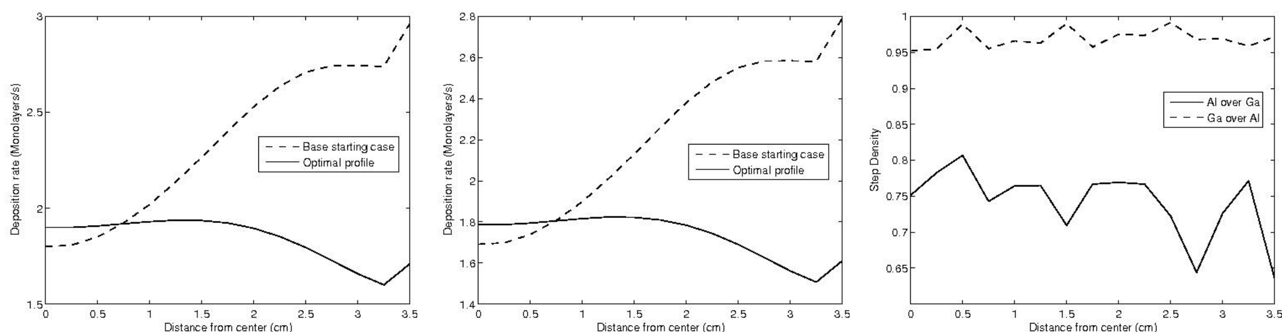

Fig. 2. Optimal deposition rate profiles for (a) AlAs over GaAs and (b) GaAs over AlAs. (c)resulting step density as a function of wafer position at optimal conditions

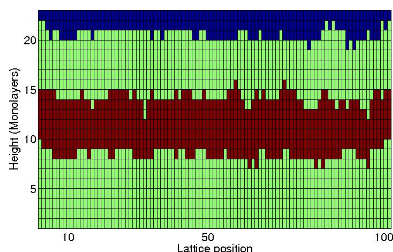

Fig. 3. Vertical slice of deposition surface at optimal conditions.

Finally, this optimization result shows the interplay between increasing temperature and obtaining improved thickness uniformity and lower step densities - these results also motivate us to consider time-varying operations and switching them when constructing different parts of the heterostructure. We also obtained substantial computational savings from employing ISAT, as approximately 8000 mesoscale evaluations were required to achieve optimal conditions. This would require about 3-4 months of simulation time, compared with the roughly 4-10 days needed using this methodology.

REFERENCES

[1] S. Raimondeau and D.G. Vlachos, "Recent developments on multiscale, hierarchical modeling of chemical reactors," *Chem. Eng. J.*, vol. 90, pp. 3–23, 2002.

[2] S. Raimondeau and D.G. Vlachos, "Low-dimensional approximations of multiscale epitaxial growth models for microstructure control of materials," *JCP*, vol. 160, pp. 564–576, 2000.

[3] A. Varshney and A. Armaou, "Multiscale optimization using hybrid PDE/kMC process systems with application to thin film growth," *Chem. Eng. Sci.*, vol. 60, pp. 6780–6794, 2005.

[4] A. Varshney and A. Armaou, "Reduced order modeling and dynamic optimization of multiscale PDE/kMC process systems," *Comp. and Chem. Eng.*, vol. 32, pp. 2136–2143, 2008.

[5] A. Varshney and A. Armaou, "Optimal operation of GaN thin film epitaxy employing control vector parameterization," *AIChE J.*, vol. 52, no. 4, pp. 1378–1391, 2006.

[6] M.A. Katsoulakis, A.J. Majda, and D.G. Vlachos, "Coarse-grained stochastic processes and Monte Carlo simulations in lattice systems," *JCP*, vol. 186, pp. 250–278, 2003.

[7] A. Armaou and I.G. Kevrekidis, "Equation-free optimal switching policies using coarse time-steppers," *Int. J. of Robust and Nonlinear Control*, vol. 15, pp. 713–726, 2005.

[8] C.W. Gear, J.M. Hyman, P.G. Kevrekidis, O. Runborg, K. Theodoropoulos, and I.G. Kevrekidis, "Equation-free multiscale computation: enabling microscopic simulators to perform system-level tasks," *Comm. in Math. Sci.*, vol. 1, pp. 715–762, 2003.

[9] C.I. Siettos, A. Armaou, A.G. Makeev, and I.G. Kevrekidis, "Microscopic/stochastic timesteppers and coarse control: a kinetic Monte Carlo example," *AIChE J.*, vol. 49, pp. 1922–1926, 2003.

[10] Y. Lou and P.D. Christofides, "Estimation and control of growth rate and surface roughness in thin film growth using kinetic Monte-Carlo models," *Chem. Eng. Sci.*, vol. 58, no. 14, pp. 3115–3129, 2003.

[11] M.A. Gallivan and R.M. Murray, "Reduction and identification methods for Markovian control systems, with application to thin film deposition," *Int. J. of Robust and Nonlinear Control*, vol. 14, pp. 113–132, 2004.

[12] S. Raimondeau, P. Aghalayam, A.B. Mhadeshwar, and D.G. Vlachos, "Parameter optimization of molecular models: Application to surface kinetics," *Ind. Eng. Chem. Res.*, vol. 42, pp. 1174–1183, 2003.

[13] A. Varshney and A. Armaou, "Identification of macroscopic variables for low-order modeling of thin film growth," *Ind. Eng. Chem. Res.*, vol. 45, pp. 8290–8298, 2006.

[14] C. Theodoropoulos, N.K. Ingle, and T.J. Mountziaris, "Computational studies of the transient behavior of horizontal MOVPE reactors," *JCG*, vol. 170, pp. 72–76, 1997.

[15] K.A. Fichthorn and W.H. Weinberg, "Theoretical foundations of dynamical Monte Carlo simulations," *JCP*, vol. 95, no. 2, pp. 1090–1096, 1991.

[16] T. Shitara, D.D. Vvedensky, M.R. Wilby, J. Zhang, J.H. Neave, and B.A. Joyce, "Step-density variations and reflection high-energy electron-diffraction intensity oscillations during epitaxial growth on vicinal GaAs(001)," *Phys. Rev. B*, vol. 46, no. 11, pp. 6815–6827, 1992.

[17] X.W. Zhou, H.A.G. Wadley, R.A. Johnson, D.J. Larson, N. Tabat, A. Cerezo, A.K. Petford-Long, G.D.W. Smith, P.H. Clifton, R.L. Martens, and T.F. Kelly, "Atomic scale structure of sputtered metal multilayers," *Acta Mater.*, vol. 49, pp. 4005–4015, 2001.

[18] F. Grosse and R. Zimmermann, "Monte Carlo growth simulation for $Al_xGa_{1-x}As$ heteroepitaxy," *JCG*, vol. 212, pp. 128–137, 2000.

[19] T. Dekorsy, M. Helm, V.A. Yakolev, W. Seidel, and F. Keilmann, "Dispersion of the nonlinear susceptibility of GaAs in the THz range," in *Opt. Soc. of America, QWB6*.

[20] S.B. Pope, "Computationally efficient implementation of combustion chemistry using in situ adaptive tabulation," *Combust. Thoery Modelling*, vol. 1, pp. 41–63, 1997.

[21] J. Xu and S.B. Pope, "Pdf calculations of turbulent nonpremixed flames with local extinction," *Combust. and Flame*, vol. 123, pp. 281–307, 2000.

[22] P. Glasserman and D.D. Yao, "Some guidelines and guarantees for common random numbers," *Management Sci.*, vol. 38, no. 6, pp. 884–908, 1992.

[23] M.A. Zazanis and R. Suri, "Convergence rates of finite-difference sensitivity estimates for stochastic systems," *Operations Res.*, vol. 41, no. 4, pp. 694–703, 1993.

[24] S.J. Chang, C.S Chang, Y.K. Su, P.T. Chang, Y.R. Wu, K.H. Huang, and T.P Chen, "Chirped GaAs-AlAs distributed Bragg reflectors for high brightness yellow-green light-emitting diodes," *IEEE Photonics Tech. Lett.*, vol. 9, no. 2, pp. 182–184, 1997.

[25] C. Cavallotti, I. Lengyel, M. Nemirovskaya, and K.F. Jensen, "A computational study of gas-phase and surface reactions in deposition and etching of GaAs and AlAs," *JCG*, vol. 268, pp. 76–95, 2004.

[26] R.H. Perry and D.W. Green, *Perry's Chemical Engineers' Handbook*, McGraw-Hill, 7th edition, 1997.

[27] J.C. Slater, "Atomic radii in crystals," *JCP*, vol. 41, no. 10, pp. 3199–3204, 1963.